A SIGNAL-TO-NOISE RATIO COMPARISON OF ULTRASONIC TRANSDUCERS FOR C-SCAN IMAGING IN TITANIUM

P.J. Howard and D.C. Copley
GE Aircraft Engines
One Neumann Way, M/D Q45
Cincinnati, OH 45215-6301

R.S. Gilmore
GE Corporate Research & Development Center
P.O. Box 8
Schenectady, NY 12301

INTRODUCTION

Digital data acquisition and the C-scan imaging of ultrasonic data offer improvements over analog recording techniques, such as strip-chart recording. As a result, peak-detected C-scan imaging is becoming the preferred method for the inspection of large titanium parts such as those found in the aircraft engine industry. The effectiveness of the inspection, however, still depends on the transducer. For this reason, a study of the effect of different transducer parameters on the sensitivity for detection of simulated defects in titanium specimens was conducted. Due to the increased emphasis on C-scan imaging, sensitivity is measured as an image-based signal-to-noise ratio.

C-SCAN INSPECTION USING FOCUSED TRANSDUCERS

NDE applications in the aircraft engine industry often require the inspection of thick (>3") segments of material to a constant sensitivity. There are currently several methods for approaching this problem including phased arrays [1], time reversal mirror imaging [2], and zoned inspection using conventional focused transducers [3]. When the latter approach is used, a series of transducers, each focused at a different depth, is used to scan the material as shown in Fig. 1. The inspection volume for each transducer is defined by its beam diameter in the focal plane and its depth-of-field. O'Niel [4] developed expressions describing the amplitude distribution around the point of focus for spherically converging pulse-echo acoustic beams. Applying similar calculations to pulse-echo, aplanatic foci (no spherical aberration), the 0.50 amplitude contour (-6 dB) defining the beam diameter, ε, is given by

$$\varepsilon = 1.03\,\lambda\left(\frac{F}{d}\right) \tag{1}$$

where d is the diameter of the transducer element, F is the focal length produced in the medium adjacent to the lens (typically a fluid such as water), and λ is the mean wavelength in the fluid. Similar expressions for the -3 dB and -1 dB beam diameters can be written simply by changing

Review of Progress in Quantitative Nondestructive Evaluation, Vol. 14
Edited by D.O. Thompson and D.E. Chimenti, Plenum Press, New York, 1995

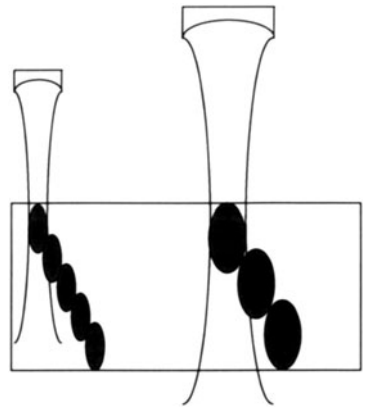

Fig. 1: Diagram illustrating the inspection of a volume of material using multiple focused transducers.

the constant in (1) to 0.74 and 0.43 respectively. The -3 dB depth-of-field, ε_z, for focused transducers operated in pulse-echo mode is given by [4]

$$\varepsilon_z = 3.6\,\lambda\left(\frac{F}{d}\right)^2\left(\frac{c_w}{c_{Ti}}\right) \qquad (2)$$

where c_w and c_{Ti} are the velocities of sound in water and titanium. Using (1) and (2), the inspection volume per ultrasonic pulse depicted in Fig. 1 can be approximated for given transducers and a zoned inspection designed.

As shown in Fig. 1, material can be inspected more rapidly using transducers with large beam diameters and depths-of-field. These transducers permit inspections with larger scan indices and fewer zones which decreases costs and increases throughput. The disadvantage of this approach is reduced inspection sensitivity. As illustrated in Fig. 2, there is a volume of material which interacts with the ultrasonic pulse at any given instant in time. This 'pulse-material interaction volume' is defined by the beam diameter and the pulse length of the ultrasound. The size of this volume controls how many grains are interacting with the sound beam at a given instant, thus affecting the level of backscatter or grain noise. High levels of grain noise can mask signals from smaller or lower acoustic reflectivity flaws which reduces the sensitivity of a given inspection. This implies a tradeoff between sensitivity and productivity which must be managed for each inspection application.

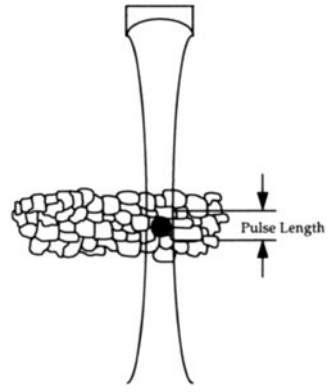

Fig. 2: Diagram illustrating the pulse-material interaction volume for a transducer.

A C-SCAN SIGNAL-TO-NOISE RATIO

There are almost as many definitions for signal-to-noise ratio (SNR) as there are applications which find the quantity useful. One which has been commonly used in industrial ultrasonics is based on the raw RF-signal at a single transducer location (Fig. 3). Here the peak of the signal plus noise, P_s, is divided by an estimate of the peak value of the noise, P_n, to form the SNR as

$$SNR = \frac{P_s}{P_n}. \tag{3}$$

A major draw back of this technique is the estimation of P_n. Typically, this estimation is done by eye from an oscilloscope using a limited number of RF-signals. This greatly limits the accuracy of the measurement.

One advantage of C-scan imaging is that it permits a more robust calculation of SNR. Since the maximum value of the grain noise has been recorded for tens-of-thousands adjacent scan positions, it should be possible to accurately estimate the maximum noise value. One approach is to use statistics to estimate a maximum noise value. When using this approach, the first step is to select a region-of-interest (ROI) from the image which contains the signal and adjacent noise. The ROI is then segmented into two regions, one which contains the signal and one containing only noise. The peak of the signal plus noise, P_s, is taken as the maximum value in the region containing the signal. Instead of trying to locate the maximum value of the noise, the mean (location), μ_n, and standard deviation (scale), σ_n, of the noise distribution are calculated using data from the noise only portion of the ROI. Then the maximum value of the noise can be estimated using $\mu_n+K\sigma_n$ where K is an appropriately chosen constant. Using this estimate for the maximum noise, the SNR can be expressed as

$$SNR = \frac{P_s - \mu_n}{(\mu_n + K\sigma_n) - \mu_n} = \frac{P_s - \mu_n}{K\sigma_n}. \tag{4}$$

Notice that μ_n is subtracted from both the numerator and denominator of (4) to remove the effect of the DC bias present in most images. To help understand this approach, consider the profile along one direction of an ROI shown in Fig. 4. This clearly illustrates the relationship of P_s, μ_n, and $\mu_n+K\sigma_n$ to each other and draws an analogy to the more traditional SNR calculation.

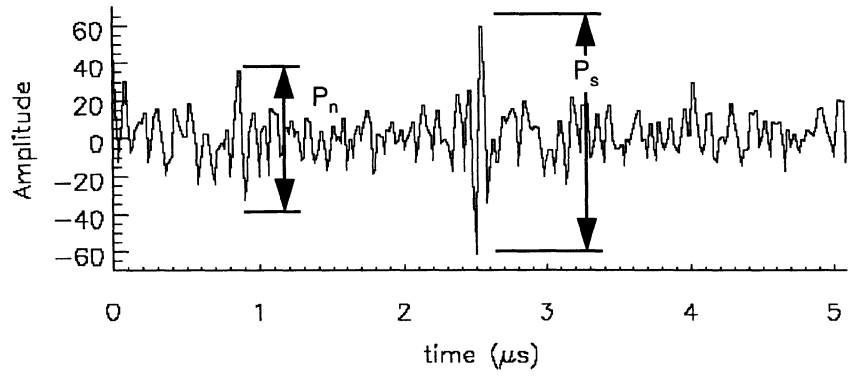

Fig. 3: Example ultrasonic A-scan illustrating the calculation of conventional or A-scan signal-to-noise ratio for a given signal, P_S.

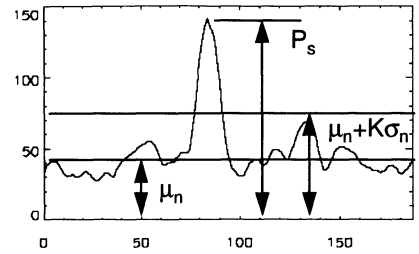

Fig. 4: Example profile through a C-scan image illustrating the calculation of a C-scan signal-to-noise ratio for a given signal, P_s.

The use of this technique implies some knowledge of the distribution of the noise. Specifically, that the noise can be accurately represented by a known statistical distribution such as the normal, lognormal or largest-extreme value distributions and that the parameters which describe the distribution can be conveniently calculated. In past work on C-scan image data, the normal distribution has been used for convenience even though it did not accurately describe the noise.[5] The results obtained by using this method, however, yielded SNR's which were more consistent with visual image quality than other methods under consideration. Far better results are obtained by using the lognormal distribution to represent the noise. Figure 5a shows a C-scan image of Ti-64 grain noise taken with a 5 MHz, F/6.0 transducer. The noise values in this image were used to calculate an experimental probability density function (PDF) for the grain noise. Next, the log mean and standard deviation of the image were found and the corresponding lognormal PDF was calculated. The two PDF's are shown in Fig. 5b. Similar calculations were performed for several different transducer and material combinations. The results shown in Fig. 5b were typical among the different combinations. In addition to the good fit to the experimental PDF's, the parameters which describe the lognormal distribution are simple to calculate. For these reasons, the lognormal distribution will be used to estimate the maximum noise and the quantities in (4) calculated accordingly.

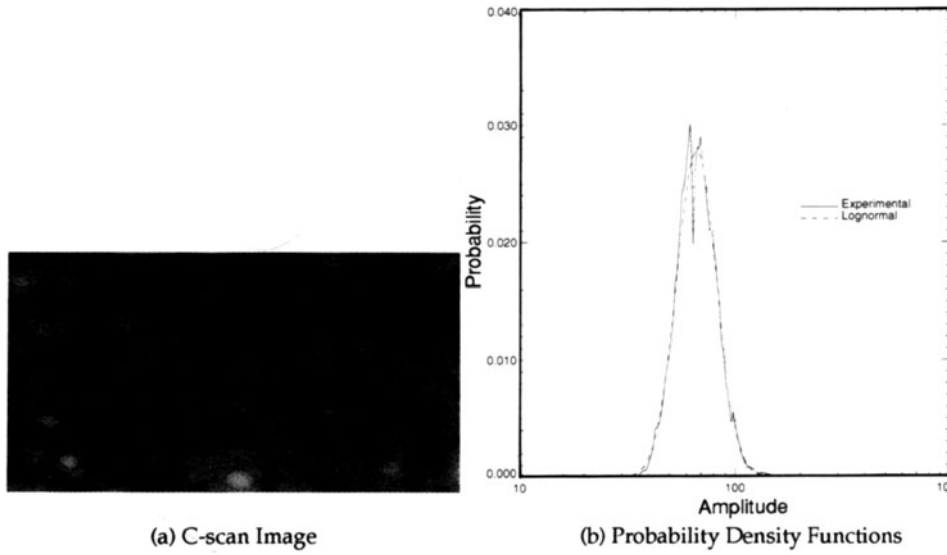

(a) C-scan Image (b) Probability Density Functions

Fig. 5: Comparison of experimental and lognormal PDF's for a C-scan image of Ti6-4 forged material.

EXPERIMENTAL RESULTS

Measurements were made using a set of transducers with varying design parameters (Table 1). Transducers were all procured from a single manufacturer, and were selected to isolate the effects of two primary design parameters: frequency and beam diameter. This was accomplished by collecting transducers where one of the parameters was held approximately constant and the other allowed to vary. The measured transducer frequencies listed in the table are experimentally determined center frequencies. The measured beam diameters are the result of averaging the -6 dB beam width in two mutually perpendicular directions from eight 1/64" (0.016") diameter flat-bottom hole (FBH) targets at 1" metal travel in a Ti6-4 sample block with the transducer focused 1" below the entry surface.

C-scan data were collected with these transducers using the sample blocks shown in Fig. 6. Each of the blocks is made from ring-rolled Ti6-4. Two of the blocks contain FBH targets of diameters 1/64" (0.016"), 2/64" (0.032"), 3/64" (0.047"), and 4/64" (0.062"). In one block, the holes were located 1" below the inspection surface and 2" below in the other. The last block contained cylindrical, uncracked, unvoided, 2.7% N, synthetic hard alpha inclusions located 1" deep [6]. These inclusions range from 2/64" (0.032") to 5/64" (0.078") in diameter and have effective reflectivities, when compared to a FBH of the same size, of less than 20%. When collecting all the C-scan images, the water path was set such that the transducer focused 1" deep in the material. In the case of the 1" metal travel targets, an 8 μs gate centered around the targets was used. For the 2" metal travel targets, a 12 μs gate was used which included both the focal zone and the far-field of the transducer. Data were collected for the 1" deep 1/64" holes, the 2" deep 1/64" and 2/64" holes, and the 5/64" and 4/64" inclusions. System attenuation settings were adjusted such that the largest target echo occupied 80-90% of the system dynamic range. From this data, SNR's for each target were calculated using (4) and the results averaged for each target size.

The results for the constant beam diameter, varying frequency transducer group is shown in Fig. 7 for both the 1" metal travel FBH's and the inclusions. These graphs show that, in general, SNR increases with frequency. The only exception occurred at frequencies below 5 MHz with the 5/64" inclusions. In this region, the wavelength of the ultrasound and the length of the inclusion (0.078") are such that there is phase-interference between the echoes from the front and the back wall of the inclusion. This phase-interference causes the increase in SNR at these lower frequencies. The results for the constant frequency, varying beam diameter transducer group are found in Fig. 8 for both the 1" metal travel FBH's and the inclusions. In this case, SNR was found to decrease for increasing beam diameter. Thus, when trying to increase sensitivity, one should consider transducers with a higher frequency and/or a smaller beam diameter.

Table 1: Nominal and measured parameters for the transducers used in the study.

Transducer	f (MHz)		d (in.)	F (in.)	ε (in.)		ε_z (in.)
	Nominal	Measured			Nominal	Measured	
A	2.25	2.3	1.5	6.0	0.107	0.096	0.4
B	3.5	3.1	1.0	6.0	0.103	0.104	0.5
C	5.0	4.5	0.75	6.0	0.097	0.100	0.7
D	5.0	4.9	1.0	6.0	0.072	0.069	0.4
E	5.0	5.1	1.25	12.0	0.116	0.116	1.0
F	5.0	4.5	1.5	18.0	0.145	0.143	1.5
G	5.0	4.7	1.5	6.0	0.048	0.050	0.2
H	7.5	6.6	0.75	9.0	0.097	0.096	1.0
I	10.0	9.2	0.75	12.0	0.097	0.096	1.4

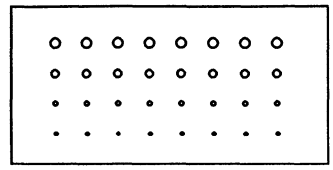

(a) 32 Flat-Bottom Hole Block

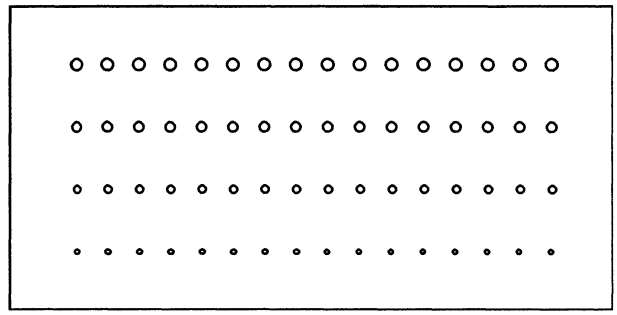

(b) 64 Inclusion Block

Fig. 6: Diagrams showing target placement for the 32 flat-bottom hole (1″ and 2″ metal travel) sample blocks and the 64 synthetic hard-alpha inclusion sample block.

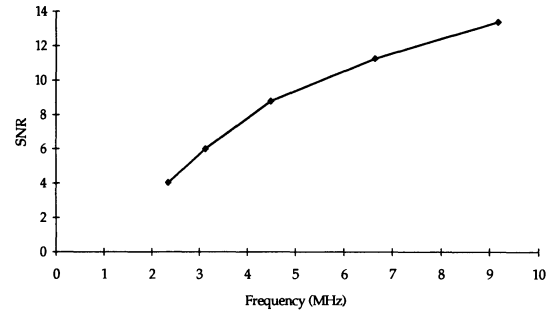

(a) Flat-Bottom Holes

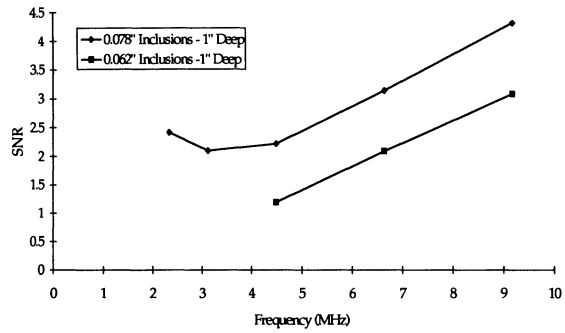

(b) Synthetic Inclusions

Fig. 7: Results for group of transducers with 0.100″ nominal beam diameter and varying frequency for 1/64″ FBH's and 5/64″ and 4/64″ synthetic hard-alpha inclusions at 1″ metal travel.

There is an additional benefit in terms of inspection productivity which can be gained by using higher frequency transducers. For a constant beam diameter, the depth-of-field increases with increasing frequency. This effect can be seen in Table 1 when considering the constant beam diameter, varying frequency transducer group. Figure 9 shows the results from imaging the 2" metal travel holes which were approximately 1" beyond the focal zones of the transducers. Here, the SNR of the targets increases with the frequency, due to the corresponding increase in depth-of-field. So, for a constant beam diameter, increasing frequency creates a larger depth-of-field which permits a volume of material to be inspected to a constant sensitivity with fewer transducers.

CONCLUSION

The effect of different transducer design parameters on the signal-to-noise ratio of planar reflectors in Ti-6-4 was investigated. Two groups of transducers were assembled: one with constant (0.100") beam diameter and varying frequency and one with constant (5 MHz) frequency and varying beam diameter. C-scan data were collected with each transducer on 0.016" and 0.032" flat-bottom holes at 1" and 2" metal travel and 0.078" and 0.062" 2.76% N cylindrical titanium hard-alpha inclusions with the transducers focused at 1" in the titanium. For all of the 1" metal travel targets, SNR increased with increasing frequency and decreased with increasing beam diameter. The targets at 2" metal travel were also found to have an increasing SNR for increasing frequency. This was due to the larger depth-of-field gained by increasing the transducer frequency while holding beam diameter constant. The results of this study need to be extended to non-planar reflectors, other titanium alloys, and parts with curved surfaces. When that is completed, the results should be some comprehensive guidelines for selecting transducers for the C-scan imaging of titanium alloys.

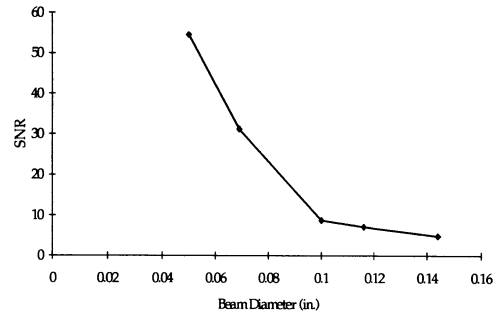

(a) Flat-Bottom Holes

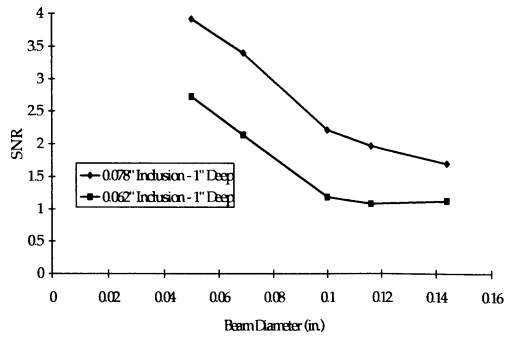

(b) Synthetic Inclusions

Fig. 8: Results for group of transducers with 5 MHz nominal frequency and varying beam diameter for 1/64" FBH's and 5/64" and 4/64" synthetic hard-alpha inclusions at 1" metal travel.

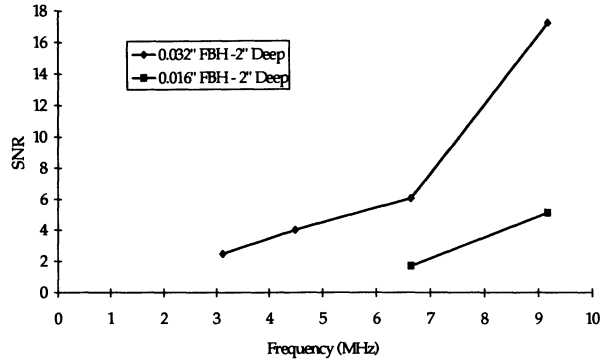

Fig. 9: Results for group of transducers with 0.100" nominal beam diameter and varying frequency for 1/64" and 2/64" FBH's at 2" metal travel.

ACKNOWLEDGMENT

This material is based upon work performed at the General Electric Company as a part of the Engine Titanium Consortium operated by ISU and supported by the Federal Aviation Administration under grant number 93-G-029.

REFERENCES

1. K. Solomon, M. Luttrell, and J. Long, *Review of Progress in QNDE, vol. 13*, eds. D.O. Thompson and D.E. Chimenti, (Plenum Press, New York, 1994), pp. 1069-1074.
2. N. Chakroun, M. Fink, F. Wu, L. Beffy, and G. Mangenet, *Review of Progress in QNDE, vol. 14*, eds. D.O. Thompson and D.E. Chimenti, (Plenum Press, New York, 1995).
3. E. Nieters, R. Gilmore, J. Young, D. Copley, P. Howard, and M. Keller, *Review of Progress in QNDE, vol. 14*, eds. D.O. Thompson and D.E. Chimenti, (Plenum Press, New York, 1995).
4. H.T. O'Neil, Journ. of Acoust. Soc. Am., vol. 21, p. 516 (1949).
5. P.J. Howard and R.S. Gilmore, *Review of Progress in QNDE, vol. 13*, eds. D.O. Thompson and D.E. Chimenti, (Plenum Press, New York, 1994), pp. 763-770.
6. M.F.X. Gigliotti, L.C. Perocchi, E.J. Nieters, and R.S. Gilmore, *Review of Progress in QNDE, vol. 14*, eds. D.O. Thompson and D.E. Chimenti, (Plenum Press, New York, 1995).